Nationaal Lucht- en Ruimtevaartlaboratorium
National Aerospace Laboratory NLR

NLR-TP-2002-320

A Quantitative Analysis of Viscous and Lift-induced Drag Components from Detailed Wake Measurements behind a Half-Span Model

F.L.A. Ganzevles, A.C. de Bruin and W. Puffert-Meissner

Nationaal Lucht- en Ruimtevaartlaboratorium
National Aerospace Laboratory NLR

NLR-TP-2002-320

A Quantitative Analysis of Viscous and Lift-induced Drag Components from Detailed Wake Measurements behind a Half-Span Model

F.L.A. Ganzevles, A.C. de Bruin and W. Puffert-Meissner*

* Deutsches Zentrum für Luft- und Raumfahrt

This report is based on a presentation held at the CEAS Aerospace Aerodynamics Research Conference, Cambridge (UK), 10-12 June 2002.

Customer:	National Aerospace Laboratory NLR
Working Plan number:	A.1.B.3
Owner:	National Aerospace Laboratory NLR
Division:	Fluid Dynamics
Distribution:	Unlimited
Classification title:	Unclassified
	June 2002

Contents

(14 pages in total)

A QUANTITATIVE ANALYSIS OF VISCOUS AND LIFT-INDUCED DRAG COMPONENTS FROM DETAILED WAKE MEASUREMENTS BEHIND A HALF-SPAN MODEL

F.L.A. Ganzevles and A.C. de Bruin
National Aerospace Laboratory (NLR)
Voorsterweg 31, 8316PR Marknesse, the Netherlands.
E-mail: ganzevle@nlr.nl, bruina@nlr.nl

W. Puffert-Meißner
German Aerospace Research Centre (DLR)
P.O. box 3267, D-38022 Braunschweig, Germany
E-mail: wolfgang.puffert-meissner@dlr.de

Abstract

In the Low Speed wind Tunnel (LST) of DNW detailed wake surveys were made behind an aircraft half-span model (ALVAST) using a rake with 5-hole probes. Different model configurations were considered including a body with wing, a body with wing and a Through Flow Nacelle (TFN) and a body with wing and a low-powered CRUF (Counter Rotating Ultra-high-bypass Fan).
The lift and drag coefficients calculated from the measured velocities and pressures in the wake are compared with the force coefficients measured with a force balance. The spanwise distributions of lift, viscous drag and induced drag are presented.

List of symbols and abbreviations

A_w	half wing planform area (0.6349 m^2)	[m^2]
A_{tun}	tunnel cross-sectional area (6.75 m^2)	[m^2]
b	full wingspan (3.44 m)	[m]
c	local wing chord	[m]
c_{avg}	average wing chord (S/b = 0.369m)	[m]
C_D	total drag coefficient (C_D = D/qS)	[-]
$C_{D,i}$	induced drag coefficient	[-]
$C_{d,i}$	local induced drag coefficient	[-]
$C_{D,p}$	viscous drag coefficient	
$C_{d,p}$	local viscous drag coefficient	[-]
$C_{D,f}$	total drag of the fuselage	[-]
$C_{ă}$	local lift coefficient	[-]
C_L	lift coefficient (C_L = L/qS)	[-]
C_{pt}	total pressure coefficient	[-]
D	drag (twice the half-model value)	[N]
D_i	induced drag	[N]
D_p	profile or viscous drag	[N]
L	lift (twice the half-model value)	[N]
p	static pressure	[Pa]
p_t	total or stagnation pressure	[Pa]
q	dynamic pressure (q = ½ ɟ V^2)	[Pa]
S	wing area (S = 2A_w = 1.270 m^2)	[m^2]
u,v,w	velocity components	[m/s or dimensionless]
V	undisturbed flow velocity	[m/s]
x,y,z	tunnel co-ordinate system (see Fig 3)	

Greek

$\breve{U}_m$	model angle of attack	[°]
ξ	threshold level for smoothing of $ϑ_x$	[1/s]
ɟ	air density	[kg/m^3]
σ	flow deceleration parameter	[1/s]
ϕ	cross-flow velocity potential	[m^2/s]
ψ	cross-flow stream function	[m^2/s]
$ϑ_x$	stream-wise vorticity	[1/s]

Subscripts

min	minimum
max	maximum

Abbreviations

ALVAST	Aerodynamische LeistungsVerbesserung An Subsonischen Transportflugzeugen
B	Body (fuselage only) configuration
BW	Body + Wing configuration
BWT	Body + Wing + TFN configuration
BWC	Body + Wing + CRUF configuration
CRUF	Counter Rotating Ultra-high-bypass Fan
DLR	Deutsche Forschungsanstalt für Luft und Raumfahrt e.V.
DNW	German Dutch Wind tunnels
FB	measured with force balance
LST	DNW Low Speed wind Tunnel
RPM	rotations per minute of the CRUF
TFN	Through Flow Nacelle
WAKE	software programme for drag and lift analysis from wake survey data
sm	sm = 1/0: with-/without threshold level smoothing (ξ) of streamwise vorticity

extr extr = 1/0: wake data are or are not extrapolated to the model symmetry plane

Introduction

Within the framework of DLR-NLR co-operation on engine/airframe integration, low speed wind tunnel tests in the DNW-LST have been conducted with a generic civil aircraft half-span-model ALVAST. The model can be fitted with wing-mounted ultra-high-bypass engines. The major objective of the tests was to obtain a better understanding of the wing nacelle interference effects and to provide a database for comparison with CFD results. The flow field behind the model has been measured in detail with a rake with eighteen 5-hole probes. A quantitative analysis of the wake flow data is possible with the method of Maskell (Ref 1), later extended and refined by Wu (Ref 2), Weston (Ref 3) and Kusunose (Ref 4). It allows the determination of the viscous and induced drag and of the lift from the measured velocities and pressures in the wake.

Examples of quantitative wake surveys are given in Refs 5-6.

In the present study wake surveys (see Refs 7-10) were made for three model configurations:

- fuselage + cruise wing (configuration code BW)
- fuselage + cruise wing + TFN (configuration code BWT)
- fuselage + cruise wing + low powered CRUF (configuration code BWC).

The CRUF was driven with pressurised air. For each configuration forces and pressures have been measured for a range of model angle of attack values and the wakes were measured in detail for three model angles of attack (α_m = 2, 4 and 6°).

In the present paper the five-hole probe rake data are processed with the computer program WAKE. This program, based on the extended method of Maskell, was developed in co-operation with the "Delft University of Technology", Faculty of Aerospace Engineering. It yields the lift and drag distributions along the wing span and allows the separate determination of viscous and induced drag components. The results are compared with the measured forces and integrated wing section pressures.

Model and test set-up

The wind tunnel tests have been conducted in the low speed wind tunnel DNW-LST. The test section is 3m wide and 2.25m high (see section view AA in Fig 1) and its length is 5.75 meter. The ALVAST half model configurations with code names B (body or fuselage alone), BW and BWT were suspended from the ceiling (see Fig 2) and connected to the platform of the external six-component overhead balance.

The model configuration with CRUF (configuration code BWC) was mounted on the tunnel floor and connected to an external balance (see Fig 3). It was tested with a RPM setting of about 3700. In this case the CRUF operates at nearly zero thrust, for comparison with the TFN configuration.

In both cases the model was fixed to a turntable to enable angle of attack variations. Between the model and the wind tunnel wall a so-called 'peniche' was used in order to limit the influence of the tunnel wall boundary layer on the measured forces. The ALVAST model is rather large: the distance between the wing tip and the tunnel wall is only about 18 percent of the test section height.

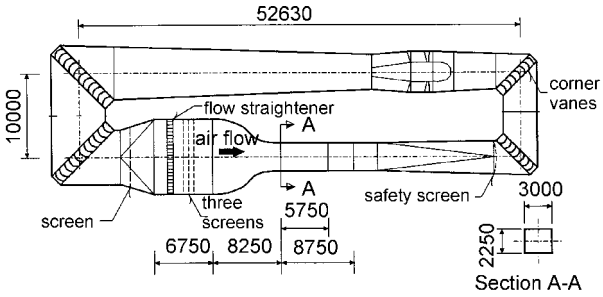

Fig 1 Sketch of the DNW-LST low speed wind tunnel circuit (dimensions in mm)

Fig 2 ALVAST Body Wing Through Flow Nacelle half-model configuration in DNW-LST

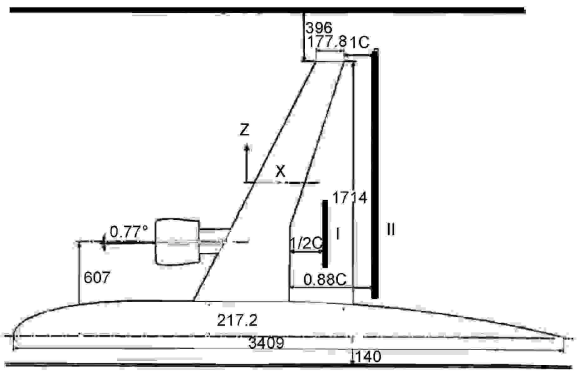

Fig 3 Schematic view of ALVAST half-model with CRUF and wake traverse planes I and II (dimensions in mm)

Tests started with the measurement of model forces and pressures followed by wake survey tests. The wake surveys were made with a five-hole rake. The three velocity-components and the total pressure losses were measured. This allows a full wake analysis with the WAKE program. Additional wake surveys were made with a pitot rake, which allows a comparison of both measurement techniques. For the body alone (B) configuration force measurements but no wake surveys have been taken.

Wing surface pressures at nine wing sections were measured as well.

Wake traverses

Complete flow fields have been measured at roughly one chord behind the tip trailing edge (location II in Fig 3). The rake has been traversed slowly (about 3.5 mm/s) in wing-normal direction over a distance q_{pz} of about 620 mm. Data points were taken roughly each second. Each traverse covers 255 mm of the wingspan. Therefore, six traverses were needed to cover the complete flow field from wing root to wing tip. Intermediate traverses were made behind the TFN/CRUF and the wing tip, because the probe-pitch (15mm) was considered too large in these areas with large spanwise gradients in the flow. Therefore in total eight rake traverses were needed to cover the domain of interest with sufficient resolution (total number of grid points about 28000, taken within about half an hour of measuring time).

Additional flow field measurements were performed behind the TFN and CRUF at about 0.5 chord distance behind the wing (location I in Fig 3). This enables to follow the downstream evolution of the complex flow field. Rake calibration (see Ref 11) yields the total pressure coefficient C_{pt}, the velocity components u, v and w and the local static pressure. Velocities are non-dimensionalised with the free-stream tunnel velocity (V = 60 m/s). The total pressure coefficient C_{pt}, the axial vorticity ω_x and the local flow deceleration parameter σ are defined as:

$$C_{pt} = (p_t - p_{t\infty}) / q \qquad (1)$$

$$\omega_x = \partial w / \partial y - \partial v / \partial z \qquad (2)$$

$$\sigma = \partial v / \partial y + \partial w / \partial z \approx - \partial u / \partial x \qquad (3)$$

It is interesting to note from Eq. 3 that (based on the continuity equation for incompressible flow) the local flow deceleration can be obtained from the measured cross-flow components in a plane x = constant.

Within wake regions C_{pt} attains negative values. In the jet of the CRUF simulator C_{pt} may attain positive values locally depending on the thrust level. Previous flow field measurements with the 5-hole rake have been reported in Ref 12.

Lift and drag definitions

The aerodynamic force coefficients are defined according to the following equations:

$$C_L = L / (\tfrac{1}{2} \rho V^2 S) = L / (qS) \qquad (4)$$

$$C_D = D / (\tfrac{1}{2} \rho V^2 S) = D / (qS) \qquad (5)$$

Lift and drag forces on the complete model are assumed equal to twice the values obtained for the half model. Local force coefficients are usually made dimensionless with the local chord. However, in order to allow a straightforward spanwise integration to total force coefficients, the local coefficients are here multiplied with a factor c/c_{avg} (c_{avg} is the average wing chord).

Processing of the flow field data with WAKE

Figure 4 gives a schematic overview of the data-processing steps of the flow field data. The wind tunnel data are processed by the LST data processing system. The resulting flow field parameters, model pressures and force balance data are saved in NLR TOUT-file format.

Quick inspection of the measured flow field data can be made with the VisuRake PV-Wave software application. Processing was done with the VeloRegu software application that combines (by re-interpolation to a regular rectangular mesh) the TOUT-data of several rake traverses into one data field. If necessary the flow field data can be extrapolated to the model symmetry plane using proper flow symmetry conditions (v = 0 and ω_x = 0) in the model symmetry plane. For the present application both extrapolated (0 < y/b < 0.53) and non-extrapolated (0.07 < y/b < 0.53) data fields were created.
In the VeloRegu processing step irregularities due to small probe-to-probe imperfections are corrected. These small imperfections have to be removed because their integration in large domains outside the actual viscous flow field may lead to considerable errors in the determination of lift and drag terms.

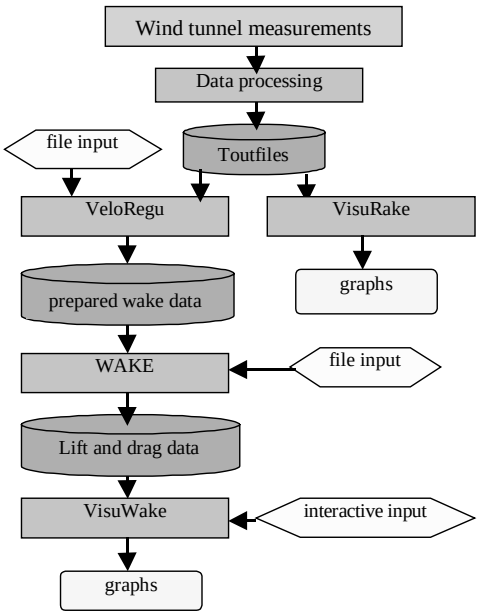

Fig 4 Overview of wake data processing steps

For obtaining correct answers for the profile drag the C_{pt} values in the regions outside of the shear layers have to remain close to zero. Residual errors were effectively removed by setting C_{pt} to zero whenever its absolute value was below a prescribed threshold value (0.02).

Similarly, small probe-to-probe variations in crossflow velocity components cause oscillations in their derivatives and thus in the streamwise vorticity (derived with first order central differencing with neighbouring (points). These in turn, when not removed, cause oscillations in the spanwise distributions of lift and especially in the induced drag (but have only a minor effect on the total integrated lift and induced drag). By simply putting the vorticity to zero when its absolute value is less than a certain user prescribed threshold level (called ξ) the oscillations in spanwise distributions could effectively be diminished. For the clean wing (BW, Λ_m = 4°) configuration different threshold levels have been tried. The effect on the spanwise distributions of lift and induced drag is shown for three threshold levels in Fig 5. Based on these test calculations with WAKE a threshold level ξ = 0.5 was chosen. This gives sufficient smoothing, while preserving total lift and drag values within 2% of the non-smoothed values.

The basic equations from Maskell's method (Refs 1-4), used in WAKE, are given in Appendix A. Inspection of results is made with VisuWake.

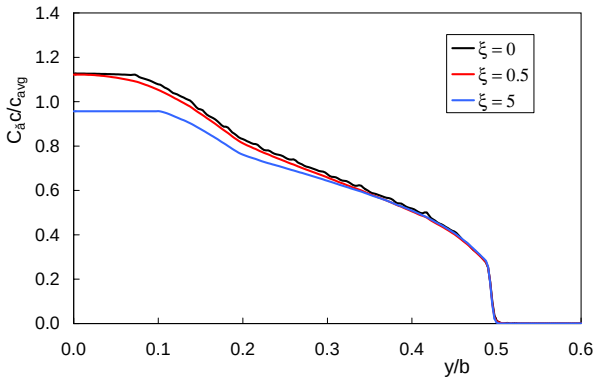

a) spanwise lift

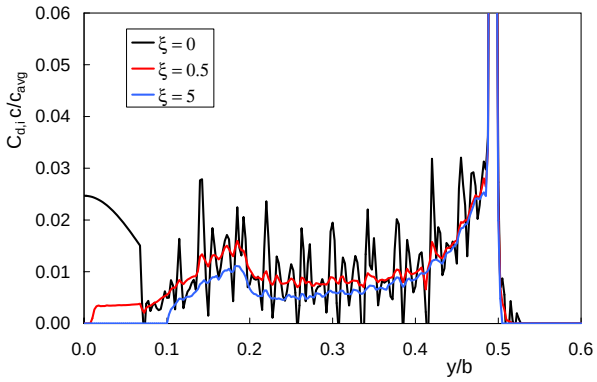

b) spanwise induced drag
Fig 5 Effect of threshold level (ξ) smoothing of streamwise vorticity ω_x

Since no complete flow fields were measured the following drag bookkeeping procedure is used:

$$C_D = C_{D,f} + C_{D,p}\big|_{extr=0} + C_{D,i}\big|_{extr=1} \qquad (6)$$

where:

- C_D is the drag coefficient.
- $C_{D,f}$ is the drag of the fuselage alone, as measured with the force balance during an alpha-sweep
- $C_{D,p}$ is the viscous drag, obtained by spanwise integration of the $C_{d,p}$ values from WAKE. This drag component is computed from the measured flow field data (*without extrapolation* to the wing symmetry plane).
- $C_{D,i}$ is the induced drag of the wing, obtained from spanwise integration of $C_{d,i}$ values from WAKE. For this drag component the flow field data were first *extrapolated* to the wing symmetry plane (assuming proper symmetry-plane conditions).

Since the wake is not fully measured, for deriving the lift a first order estimate is to assume that the inboard wing loading remains equal to the loading at the y_{min} position of the measured domain. However, here the lift and spanwise loading have been determined with the wake flow extrapolated to the wing symmetry plane. This leads effectively almost to the same result.

However, details of the actual lift carry-over and the wing fuselage interference effects on drag and lift can not be taken into account with this pragmatic procedure.

The test programme

All measurements have been carried out at M = 0.18 (V ≈ 60 m/s). The test programme is described in detail in Refs 7-8 and test results have also been reported in Ref 9. An analysis of the wake data is presented in Ref 10. During phase 1 the clean wing (BW) and the configuration with Through Flow Nacelle (designated as BWT configuration) were tested and during phase 2 the model was tested with CRUF for two power settings: RPM = 3700 and 10500. Only the low-power CRUF setting (denoted as BWC) will be considered here. During each test campaign two types of measurements were performed:

- force balance and model pressures
- 5-hole rake traverses (pitot rake traverses were made as well, but are not considered here)

The lift and drag force coefficients C_L and C_D were obtained from the force balance data and are compared with the WAKE results.

Some measurement results

Some typical flow field measurement results are shown here. Examples of streamwise vorticity ϖ_x fields, shown together with (some of) the measured cross-flow vectors, are given in Figs 6a,b for the BW and BWT configuration at α_m = 4°.

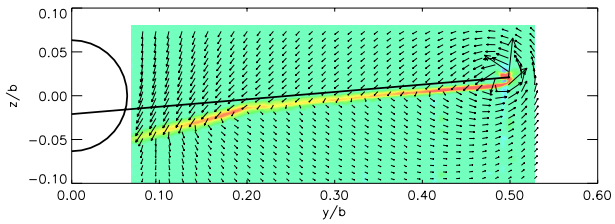

a) BW configuration

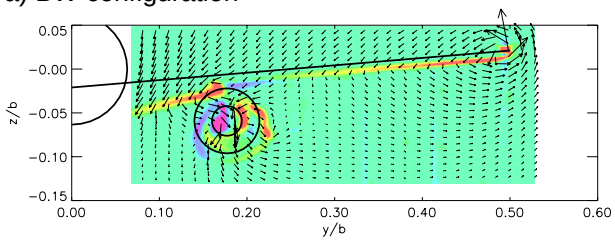

b) BWT configuration

Fig 6 Some measured vorticity fields and cross-flow velocity vectors (α_m = 4°, position II)

The model wing trailing edge position (for α_m = 0° !) is indicated for reference in the same figure. The spanwise velocity component clearly changes sign across the thin wake (vorticity layer) of the wing. Peak vorticity values occur in the evolving wing-tip vortex. For the BW configuration a “kink” in the wake position occurs near the kink in the wing planform at y/b = 0.2. For the BWT configuration the vorticity in the wing wake becomes *negative* just outboard from the TFN and becomes again positive for y/b > 0.23. The flow behind the TFN is quite complex as can be seen from Figs 7a,b. Large total pressure losses occur in the TFN core region. The core region is surrounded by the wake of the TFN cowl. Flow details like the wakes from the outer cowl supporting struts are clearly visible. The corresponding vorticity field and cross-flow vectors are shown in Fig 7b. For the BW configuration the vorticity in the wing wake is always positive, whereas the vorticity in the wing wake outboard from the TFN becomes locally negative. This points to a significant change in wing loading in the region near the TFN (with similar behaviour for the BWC configuration).

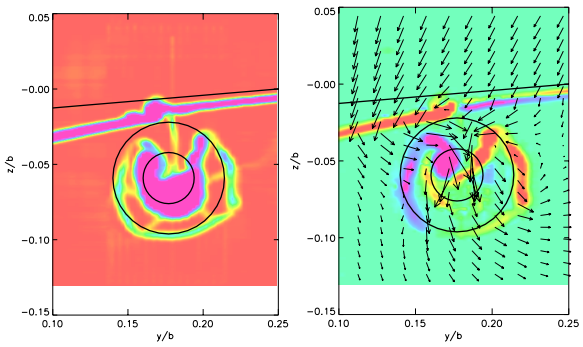

a) C_{pt} b) vorticity, ω_x

Fig 7 Measured pressure loss C_{pt} and vorticity ω_x (BWT configuration, α_m = 4°, position I)

Measured C_{pt} losses from 5-hole rake at wake positions I and II and from the pitot rake at wake position II are compared in Fig 8. A cross-section through the wake of the clean wing (BW) configuration is shown. The spreading of the wake downstream and the decrease in maximum pressure loss C_{pt} is clearly visible. A good agreement between both measurement techniques is observed.

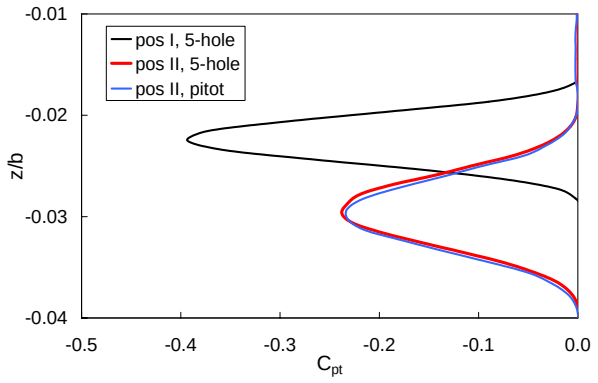

Fig 8 Measured pressure loss C_{pt} at y/b = 0.15 for BW configuration (positions I and II, α_m = 4°)

Lift analysis

Figures 9 and 10 show spanwise wing load distributions for the BW and the BWC model configurations. Each figure shows results for the three model angle of attack settings. The symbols denote the wing loading as obtained by integration of the wing pressure sections and the lines show the results obtained from integration of stream-wise vorticities with the WAKE program (see Eq A.19). For the BW (clean wing) configuration the WAKE results are somewhat below the results from the pressure integration. For the BWC configuration the integrated wing pressures indicate a decrease in *wing*-loading near the CRUF, compared to the BW case. A similar behaviour is found for the BWT configuration. It should be noted that gradients in the spanwise *wing*-loading are directly related to the local vorticity levels in the *wake of the wing.* It has already been noted in Figs 6b and 7b that vorticities with opposite sign occur in the wing wake region outboard of the TFN (and also of the CRUF), which points to a decrease in wing loading in the region outboard from the CRUF. Confining the regions of integration for the WAKE program to either the wake region of the wing alone or to the CRUF (the thin lines shown in Fig 10 for the α_m = 4° case) indeed confirms the decrease in wing loading in the CRUF region. At the same time the CRUF is seen to carry some additional lift.

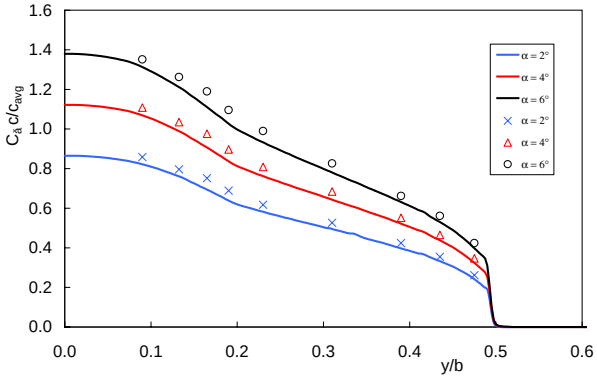

Fig 9 Spanwise lift distribution for BW configuration computed with WAKE (lines) and from wing pressure sections (symbols)

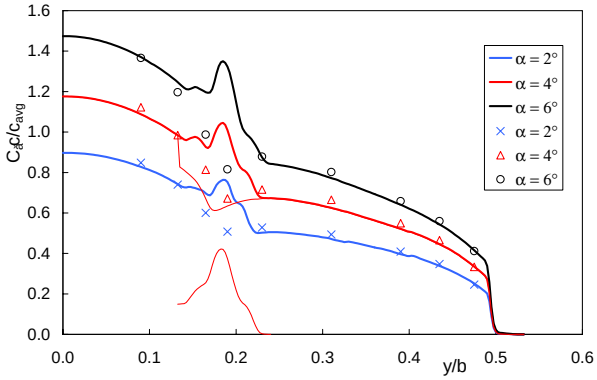

Fig 10 Spanwise lift distribution for BWC configuration computed with WAKE (lines) and from wing pressure sections (symbols).

The computed total lift coefficients from WAKE are compared with the uncorrected force balance results in Figs 11a-c. In the same figure also the result from the integrated wing section pressure sections is shown (for the latter a constant inboard wing loading has been assumed). It is concluded

that for the BWC configuration the WAKE results are close to the force balance results, whereas for the BW and BWT configuration the WAKE results are somewhat lower.

Note that in this study classical tunnel wall corrections were not yet applied to the force data.

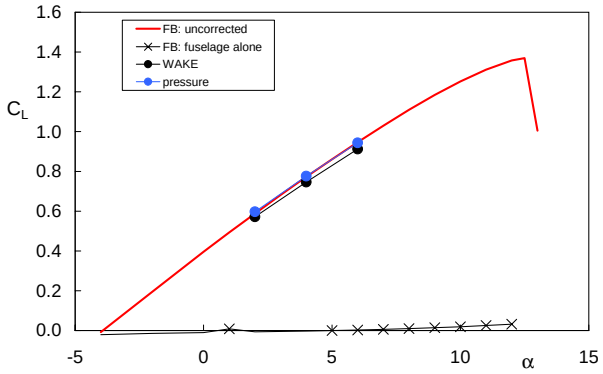

a) BW configuration

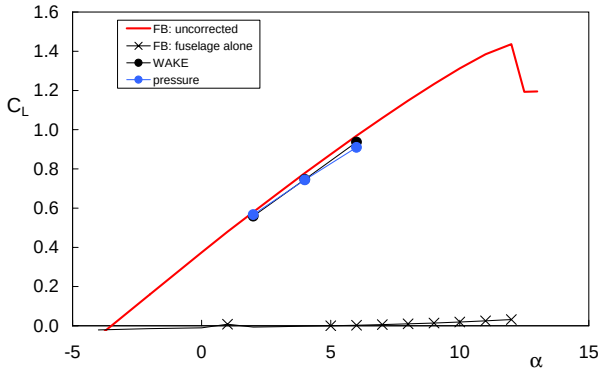

b) BWT configuration

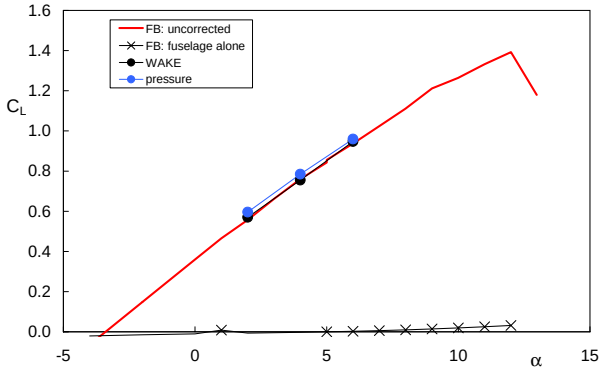

c) BWC configuration

Fig 11 Comparison of force balance, WAKE and integrated wing section pressure total lift coefficients C_L.

Profile or viscous drag

Spanwise distributions of the viscous or profile drag $C_{d,p}$ were determined with the WAKE program. Fig 12 shows as an example results for the BW configuration for α_m = 2, 4 and 6°. The profile drag slowly increases with the model angle of attack. The dip in the viscous drag near the wing root and near the kink in wing plan form (y/b=0.2) are to be noted. A relatively small contribution to the profile drag relates to the wing tip vortex.

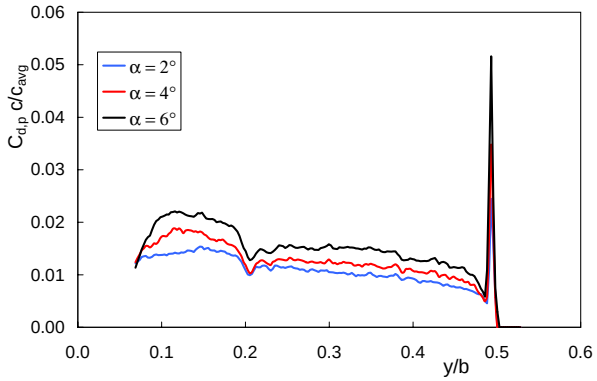

Fig 12 Spanwise viscous drag distribution for BW configuration

A comparison of $C_{d,p}$ values for different model configurations at α_m = 4° is shown in Fig 13. It is obvious that for the BWC and especially the BWT configuration a considerable contribution to the profile drag is coming from the wake of the CRUF or the TFN.

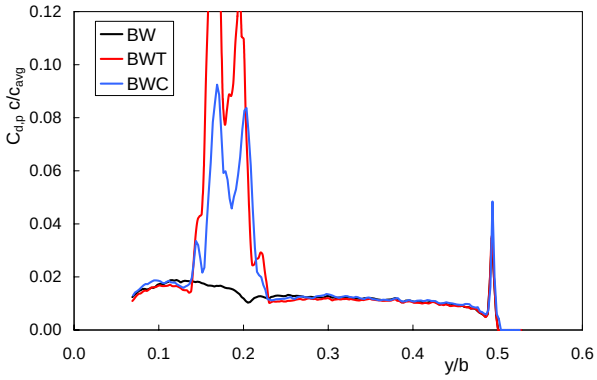

Fig 13 Spanwise viscous drag distribution at α_m=4°

Induced drag

The induced drag component is evaluated with WAKE, using the extended Maskell method of Wu (Ref 2). The measured flow fields were first extrapolated to the model symmetry plane (insisting on suitable symmetry conditions) and

zero streamwise vorticity was assumed in the regions above, below and to the right of this area. Determination of the induced drag requires the solution of a Poisson equation for the cross-flow stream function ψ and the velocity potential ϕ. Since the tunnel wall and the symmetry plane are to be considered as a streamline, Dirichlet boundary conditions (ψ=0) are applied, details are given in Appendix A. For its solution WAKE employs (just as in Ref. 6) a standard finite difference procedure from FISHPACK. An alternative method (based on Green function approach) will be implemented in near future.

It was found that the contribution of the cross-flow velocity potential term ϕ to the induced drag was negligibly small. An iso-contour plot of the stream function ψ for the BW configuration at α_m = 4° is shown in Fig 14a and for the BWC configuration it is shown in Fig 14b. The stream function ψ is seen to increase steadily from the model symmetry plane and attains maximum values near the wing tip vortex position. Some deformations in the iso-contour plot for ψ are noticeable in the CRUF region. The integrand for the lift induced drag calculation (see Eq A.16) is equal to $\psi\omega_x$.

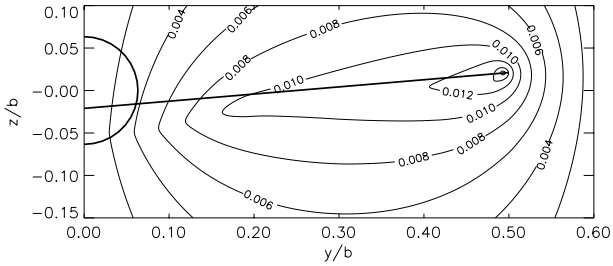

a) BW configuration

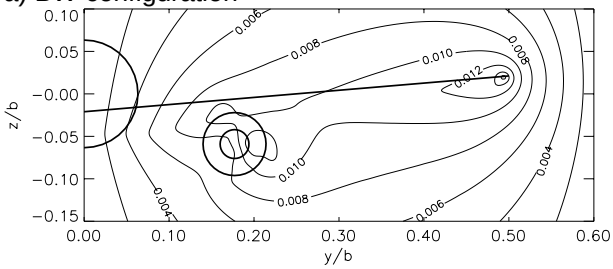

b) BWC configuration

Fig 14 Computed stream functions ψ (α_m = 4°)

For the BW configuration spanwise distributions of the induced drag $C_{d,i}$ are shown in Fig 15. The induced drag increases (of course) with model angle of attack. The wing-tip region and the region just in-board from the kink in wing plan-form contribute more than average to the induced drag. The latter can be understood because of local variation in the spanwise load distribution in this area (see also Fig 9).
As a result of the wake roll-up process vorticity becomes concentrated in the vortex core when moving downstream in the wake. Therefore, from Eqs A.15c and A.16, contributions to the induced drag will become progressively concentrated in the vortex core. At the investigated wake position II, already a considerable part of the induced drag is found in the vortex core.

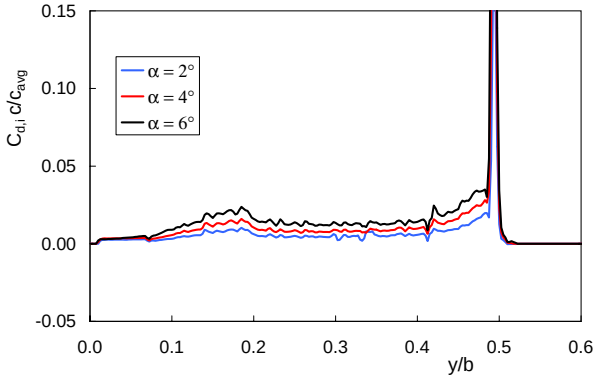

Fig 15 Spanwise induced drag distributions for BW configuration

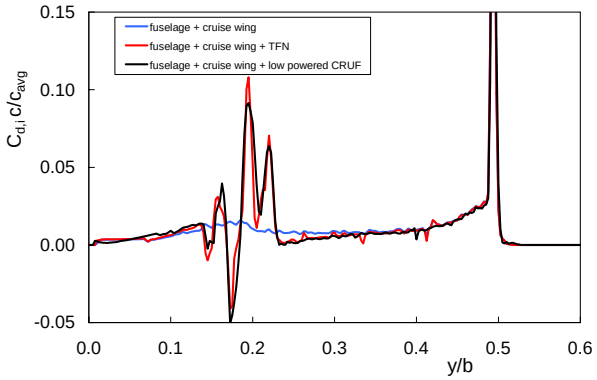

Fig 16 Spanwise induced drag distributions for BW, BWT and BWC configuration at α_m = 4°

A comparison of spanwise induced drag ($C_{d,i}$) distributions for different model configurations at α_m = 4° is shown in Fig 16. When comparing the BWT and BWC results with the BW result it is observed that the contribution to the induced drag of the region outboard from the TFN or CRUF has become significantly less. Near the TFN and CRUF both positive and ***negative*** contributions to the induced drag are found. The negative contributions come from local areas with negative vorticity and positive ψ (see Eq A.16).

Total drag

The total drag terms from WAKE are compared with the uncorrected force balance results in Fig 17a-c. For the total drag a good agreement is observed with the uncorrected force balance data, especially for the BW and BWT configurations.

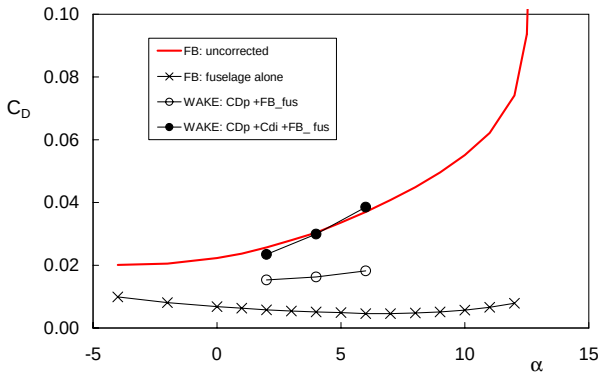

a) BW configuration

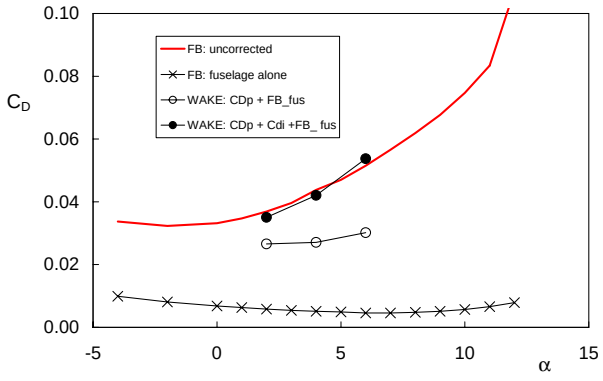

b) BWT configuration

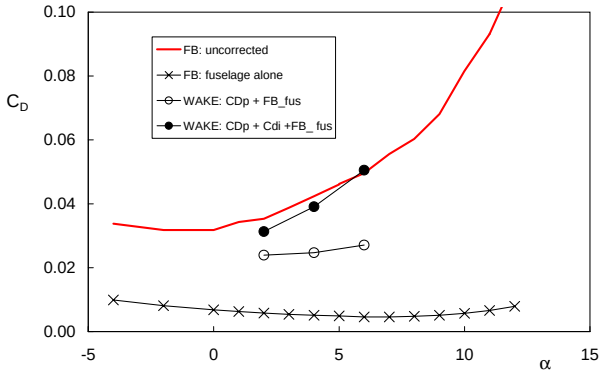

c) BWC configuration

Fig 17 Comparison of computed and measured (force balance) C_D values

For the BWC configuration the increase of viscous or profile drag with model angle of attack seems different than for the BW and BWT configurations.

Grid size sensitivity

All data processing with WAKE has been done on a grid that is close to the grid resolution of the measurements ($\Delta y/b = 0.0025$ and $\Delta z/b = 0.0010$). Data processing on a finer grid is of no value because it requires linear interpolation in the measurement data. In order to see how sensitive the results are for the grid size some additional calculations were made. For the clean wing configuration at $\alpha_m = 4°$ the original data were re-interpolated to a two and even four times coarser grid (in both directions). No important effect was found on the total drag components (see Table 1). This is rather surprising, because with the coarsest grid there are only about 5 grid points across the wake! This is however no advertisement for using coarse measurement grids, because inspection of the spanwise distributions shows a clear degradation of these data.

Table 1 Effect of grid size used in WAKE on the computed viscous and induced drag

$\Delta y/b \times \Delta z/b$	$C_{D,p}$	$C_{D,i}$
0.0025×0.001	0.01116	0.01367
0.0050×0.002	0.01104	0.01398
0.0100×0.004	0.01088	0.01392

Conclusions

A ***qualitative*** inspection of the measured flow-field data showed interesting details of the flow development:

- the thickening of the wakes with increasing angle of attack,
- changes in the flow with downstream position in the wake and with model angle of attack. In particular for the complex flow downstream of the TFN and CRUF
- the wing wake in the region just outboard of the TFN or CRUF is considerably modified. It locally carries negative vorticity due to the presence of the nacelle.

A ***quantitative*** analysis of the 5-hole rake flow field data with the programme WAKE showed:

- good agreement of spanwise wing loading derived from the wake data and the integrated wing section pressures,
- good agreement between the total lift values obtained with WAKE and the total lift values from the force balance,

- interesting information for the spanwise distributions of viscous and induced drag contributions,
- good agreement between the total drag values obtained from WAKE and the total drag values from the force balance,
- weak sensitivity to the grid size used in WAKE.

The present test set-up only allowed the measurement of part of the wake (aside from the fuselage). For the lift and drag analysis with WAKE it was then needed to make assumptions on the drag of the fuselage. The force balance results of the fuselage alone test were simply added to the wing drag derived with WAKE. This procedure does not take into account the actual drag interference effects between the wing and the fuselage.

It should further be noted that the present wind tunnel model is rather large for the LST test section. So both the WAKE and the force balance data will need considerable corrections for the presence of the tunnel walls. For the present comparison of WAKE and uncorrected force balance results these corrections were, however, not needed.

Finally, a satisfactory agreement between the measured C_{pt} values with 5-hole rake and pitot rake was observed.

References

1. E.C. Maskell: *Progress towards a method for the measurement of the components of drag for a wing of finite span*, RAE Technical Report 72232, 1972.
2. J.C. Wu; J.E. Hackett; D.E. Lilley: *A generalised wake integral approach for drag determination in three-dimensional flows*, AIAA 79-0279, Jan. 1979.
3. R.P. Weston: *Refinement of a method for determining the induced and profile drag of a finite wing from detailed wake measurements*, PhD Thesis University of Florida, USA, 1981.
4. K. Kusunose: *Drag prediction method based on a wake-integral method,* AIAA 98-2723, pp. 501-514, 1998.
5. A.J. Priest; D.G. Dobney; R.P. Hill: *Measurements in the near-wake of a transport model, to determine the lift, drag and drag components using Maskell's analysis*, RAE TP81012, February 1981.
6. G.W. Brune: *Quantitative low-speed wake surveys*, Journal of Aircraft, vol. 31, no. 2, pp. 249-255,1994.
7. G.H. Hegen: *Test report of force and flowfield measurements on the ALVAST half model in the low speed wind tunnel LST, Phase 1, Test number 5619,* NLR TR 96576.
8. G.H. Hegen: *Test report of force and flow field measurements on the ALVAST half model supplied with turbo-powered CRUF simulator in the low speed wind tunnel DNW-LST, Phase 2, Test Number: 6628*, NLR-TR-2000-701.
9. G.H. Hegen; W. Puffert-Meissner; L. Dieterle; H. Vollmers: *Flow field investigations on a wing installed Counter Rotating Ultra-high-bypass Fan engine simulator in the low speed wind tunnel DNW-LST*, NLR-TP-99104.
10. A.C. de Bruin; F.L.A. Ganzevles; W.B. de Wolf: *Drag and lift analysis from wake surveys behind the ALVAST half-model. Clean wing, through flow nacelle and turbo-powered CRUF simulator model configurations*, NLR-TR-2002-116.
11. E.M. Houtman and W.J. Bannink: *The calibration and measuring procedure of a five hole hemispherical head probe in compressible flow*, TU Delft Report LR-585.
12. A.C. de Bruin; G.H. Hegen; P.B. Rohne; Ph. R. Spalart: *Flow field survey in trailing vortex system behind a civil aircraft transport model at high lift*, NLR TP 96284 (paper presented at AGARD symposium on *The characterisation and modification of wakes from lifting vehicles in fluids*, Trondheim, 20-23 May 1996).

Appendix A: Equations

From local measurements of velocities and pressures in the wake of a wing or model the drag and lift can be determined. A spanwise distribution of lift or drag is also possible to obtain from these data. The method is based on Maskell (Ref 1).
The drag, D, is given by:

$$D = \iint \left(p_1 + \rho u_1^2\right) dS - \iint \left(p_2 + \rho u_2^2\right) dS \qquad (A.1)$$

The suffices 1 and 2 refer to upstream and downstream planes, respectively.
The total head relation is given by:

$$p_t = p + \frac{1}{2}\rho\left(u^2 + v^2 + w^2\right) \qquad (A.2)$$

The total head **outside the boundary layer and wake** is directly related to the total head far upstream:

$$p_t = p_{t0} = p_0 + \frac{1}{2}\rho u_0^2 \tag{A.3}$$

with the suffix 0 indicating the undisturbed flow far upstream. Substitution of p from A.2 and $p_{t1} = p_{t0}$ from A.3 the drag relation A.1 becomes:

$$D = \iint_{wake}(p_{t0} - p_{t2})dS + \frac{1}{2}\rho\iint\left(u_1^2 - u_2^2\right)dS + \\ + \frac{1}{2}\rho\iint\left(\left(v_2^2 + w_2^2\right) - \left(v_1^2 + w_1^2\right)\right)dS \tag{A.4}$$

Betz introduced the velocity u^* according to $p_{t0} = p + \frac{1}{2}\rho\left(u^{*2} + v^2 + w^2\right)$, which leads to:

$$u^* = \sqrt{-u_0^2 \cdot C_{pt} - u^2} \tag{A.5}$$

So that the velocity field is the same in the true flow except in the wake. So formally:

$$\iint\left(u_0^2 - u^2\right)dS = \iint\left(u_0^2 - u^{*2}\right)dS + \\ + \iint_{wake}\left(u^{*2} - u^2\right)dS \tag{A.6}$$

The second term of RHS of equation A.6 is nonzero in the wake and the first integral of the RHS can be rewritten as:

$$\iint\left(u_0^2 - u^{*2}\right)dS = 2u_0\iint\left(u_0 - u^*\right)dS + \\ + \iint\left(u^* - u_0\right)^2 dS \tag{A.7}$$

Due to continuity[1], $\iint u_0 dS = \iint u dS$, so the first term at RHS of equation A.7 reduces to:

$$\iint\left(u_0 - u^*\right)dS = -\iint_{wake}\left(u^* - u\right)dS \tag{A.8}$$

Then with A.7 substituted in equation A.6 and the perturbation velocity, $\tilde{u}$, defined as the difference of the Betz velocity and the true axial velocity, $\tilde{u} = u^* - u_0$, it becomes:

$$\iint\left(u_0^2 - u^2\right)dS = \iint_{wake}\left(u^* - u\right)\left(u^* + u - 2u_0\right)dS + \\ - \iint\tilde{u}^2 dS\,) \tag{A.9}$$

In the same manner the second integral at RHS of A.4 is rewritten as:

$$\frac{1}{2}\rho\iint\left(u_1^2 - u_2^2\right)dS = \frac{1}{2}\rho\iint\left(u_0^2 - u_2^2\right)dS + \\ - \frac{1}{2}\rho\iint\left(u_0^2 - u_1^2\right)dS \tag{A.10}$$

Relation A.9 is substituted in A.10 and gives:

$$\frac{1}{2}\rho\iint\left(u_1^2 - u_2^2\right)dS = \\ \frac{1}{2}\rho\iint_{wake}\left(u_2^* - u_2\right)\left(u_2^* + u_2 - 2u_0\right)dS + \\ + \frac{1}{2}\rho\iint\left(\tilde{u}_1^2 - \tilde{u}_2^2\right)dS \tag{A.11}$$

The drag relation becomes:

$$D = \iint_{wake}(p_{t0} - p_{t2})dS + \\ + \frac{1}{2}\rho\iint_{wake}\left(u_2^* - u_2\right)\left(u_2^* + u_2 - 2u_0\right)dS + \\ + \frac{1}{2}\rho\iint(\tilde{u}_1^2 - \tilde{u}_2^2)dS + \\ + \frac{1}{2}\rho\iint\left(\left(v_2^2 + w_2^2\right) - \left(v_1^2 + w_1^2\right)\right)dS \tag{A.12}$$

The first three integrals at RHS of the drag relation A.12 are related to the profile drag and the fourth integral is related to the lift induced drag. The third integral is a wind-tunnel blockage correction term ΔD. According to Ref 1 it can be replaced with an integral over the wake only:

$$D_{p,2} = \Delta D = \frac{1}{2}\rho\iint\left(\tilde{u}_1^2 - \tilde{u}_2^2\right) \\ = -\rho\tilde{u}_b\iint_{wake}\left(u_2^* - u_2\right)dS \tag{A.13}$$

Where $\tilde{u}_b$ represents a uniform blockage velocity, defined as:

$$\tilde{u}_b = \frac{1}{2A_{tun}}\iint_{wake}\left(u_2^* - u_2\right)dS \tag{A.14}$$

[1] Strictly this is not valid with a powered CRUF because some extra air is added to the tunnel flow. However, estimated effect is negligibly small.

A_{tun} is the tunnel cross-sectional area. In the programme WAKE ΔD is calculated and for the present model configurations it is typically about equal to 0.0001 (so less then 0.05% of the total drag). Now with $u_e = u_0 + \tilde{u}_b$ being the *effective* velocity of the wind-tunnel stream, the two contributions to drag become:

$$D = D_p + D_i \qquad \text{(A.15a)}$$

$$D_p = \iint_{wake} (p_{t0} - p_{t2})\,dS + \frac{1}{2}\rho \iint_{wake} (u_2^* - u_2)(u_2^* + u_2 - 2u_e)\,dS \qquad \text{(A.15b)}$$

$$D_i = \frac{1}{2}\rho \iint \left((v_2^2 + w_2^2) - (v_1^2 + w_1^2)\right) dS \qquad \text{(A.15c)}$$

As shown in Refs 1-3 the equation for the induced drag can be replaced by an equation involving integration over the wake only. The derivation is rather long and will not be repeated here. Following Refs 1-3, the method used in WAKE is based on the following equations:

$$D_i = \frac{1}{2}\rho \iint_{wake} \psi \omega_x \,dy dz - \frac{1}{2}\rho \iint_{wake} \phi \sigma \,dy dz \qquad \text{(A.16)}$$

The stream function ψ is solved from a Poisson equation with the axial vorticity as source term:

$$\frac{\partial^2 \psi}{\partial y^2} + \frac{\partial^2 \psi}{\partial z^2} = -\omega_x \qquad \text{(A.17)}$$

and the velocity potential function ϕ, follows from:

$$\frac{\partial^2 \phi}{\partial y^2} + \frac{\partial^2 \phi}{\partial z^2} = \sigma \qquad \text{(A.18)}$$

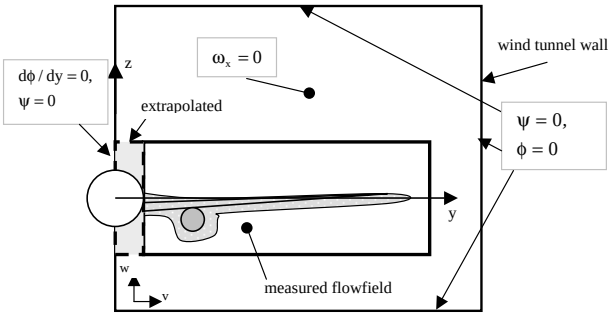

Fig A-1: The boundary conditions applied to stream-function Ψ and velocity potential ϕ.

Equations A.17 and A.18 are solved on an extended flow field covering the entire tunnel cross section. Zero vorticity is assumed in the regions above, below and to the right of the measured flow field. The solutions are subject to the boundary conditions shown in Fig A-1. It should be noted that in practice the second term of equation A.16 is much smaller than the first term and could have been neglected.

The lift, L, follows from a surface integral of axial vorticity and a surface integral involving the down-wash in the wake (see Refs 1-3 for the derivation):

$$L = \rho u_e \iint_{wake} \omega_x y\,dS + \rho \iint_{wake} (u_2^* - u_2) w_2\,dS \qquad \text{(A.19)}$$

With a 5-hole probe all necessary variables for the drag and lift analysis are available.